



Multi-temporal morphological analysis coupled to seismic survey of a mass movement from southern Italy: a combined tool to unravel the history of complex slow-moving landslides

Dario Gioia¹ · Giuseppe Corrado² · Antonio Minervino Amodio¹ · Marcello Schiattarella²

Received: 15 May 2023 / Accepted: 18 June 2024
© The Author(s) 2024

Abstract

Impressive and large-scale slow-moving landslides with a long-term evolutionary history of activity and dormancy are a common landform in the southern Apennines mountain belt. The spatial and temporal evolution of a multi-stage complex landslide located in a catchment of the frontal sector of the southern Apennine chain was reconstructed by multi-temporal geomorphological analysis, near-surface seismic survey, and DEM comparison. The Tolve landslide shows a multi-decadal evolution characterized by intermittent periods of activity and dormancy. Geomorphological evidences suggest that the initial failure of the large-scale landslide has a multi-millennial age and can be related to a roto-translational movement that evolved in an earthflow. Recent evolution is associated with a major reactivation event in the middle and lower sectors of the larger complex landslide, which probably is related to a heavy rainfall event occurred in January 1972. Recent evolution is mainly associated with minor movements in the source area, toe advancements, and wide-spread shallow landslides along the flank of the earthflow. Our results demonstrate the need to integrate traditional geomorphological analysis with multi-source data to reconstruct the evolution of slow-moving landslides and to identify their main predisposing and triggering factors.

Keywords Landslide map · Landslide reactivation · Dem of difference (DoD) · Seismic survey · Multicomponent MASW · Thrust tectonics · Southern Italy

✉ Dario Gioia
dario.gioia@cnr.it

¹ Consiglio Nazionale delle Ricerche - ISPC, C/da S. Loja, 85050 Tito Scalo, PZ, Italy

² DICEM, Università della Basilicata, Via Lanera, 75100 Matera, Italy

1 Introduction

Multitemporal geomorphological analysis and mapping of landslide-related landforms on unstable slopes are crucial, but often underestimate, activities to investigate the spatio-temporal evolution of slow-moving landslides, identify predisposing and triggering factors and plan mitigation actions (Soeters and van Westen 1996; van Westen and Lulie Getahun 2003; Giordan et al. 2013; Spalluto et al. 2021). Although recent technological advances in space and drone platforms have facilitated the quantitative analysis of short-term landslide evolution and kinematics (Calò et al. 2012; Casagli et al. 2017; Di Maio et al. 2018; Mazzanti et al. 2021; Mercuri et al. 2023), comprehensive study of large slow-moving landslides with a long-term history of intermittent dormancy and activity requires a multidisciplinary and multi-source approach where innovative remote-sensing techniques need to be integrated by traditional geomorphological analysis based on multitemporal analysis of historical images and multi-year DEM comparison (van Westen and Lulie Getahun 2003; Giordan et al. 2013; Santangelo et al. 2022). Moreover, the availability of several parameters such as slip surface depth, deformation measurements, and/or water circulation can strongly support the interpretation of the spatial/temporal evolution of mass movements and the detection of predisposing and triggering factors (Samyn et al. 2012; Di Maio et al. 2018; Hu et al. 2020; Whiteley et al. 2020; Peduto et al. 2021).

The landscape of the southern Apennine chain is locally featured by widespread landslide phenomena of different sizes and mechanisms (see for example Parise and Wasowski 1999; Parise et al. 2012; Pisano et al. 2017; Lazzari et al. 2018), especially in some sectors where the peculiar combination of litho-structural and topographic features (i.e.: high relief, outcrops of clay-rich deposits with a high degree of tectonization, presence of tectonic lineaments) have favoured the occurrence of impressive and large-scale landslides with a late Quaternary history of alternating periods of activity and dormancy (Santangelo et al. 2013; Cotecchia et al. 2015; Lazzari and Gioia 2016; Ardizzone et al. 2023). Since the Middle Pleistocene, litho-structural setting, relief growth, and tectonic setting have promoted the formation of landslide-prone landscapes in several sectors of the frontal sector of the Campania-Lucania Apennine (Fig. 1). Locally, this sector exhibits a landslide density higher than the 70%, a complex superimposition of deep-seated and shallow landslides of different size, type and kinematics and can represent suitable study areas for the investigation of the evolution and dynamics of complex unstable slopes. In this work, we investigated the multi-decadal evolution of an impressive complex landslide located in the frontal sector of the southern Apennines chain, (Italy) by using geomorphological analyses, UAV-based short-term monitoring, and near-surface seismic prospections.

The study area (Fig. 1) includes an unstable slope located near Tolve, a small town located about 10 km to the east of Potenza City (Basilicata, southern Italy). The slope is interested by a complex landslide (hereinafter Tolve landslide) showing a high variability of its active sectors in space and time. It shows clear geomorphological evidences of rotational movements in the higher-altitude sectors, whereas the lower sectors exhibit a typical pattern of an earthflow. The complex landslide is featured by limited and shallow movements in its upper sectors, whereas topographic signs of younger activity can be recognized in the middle and lower sectors of the larger landslide. Such an active sector shows geomorphological features typical of an earthflow such as a main arcuate scarp, a narrower

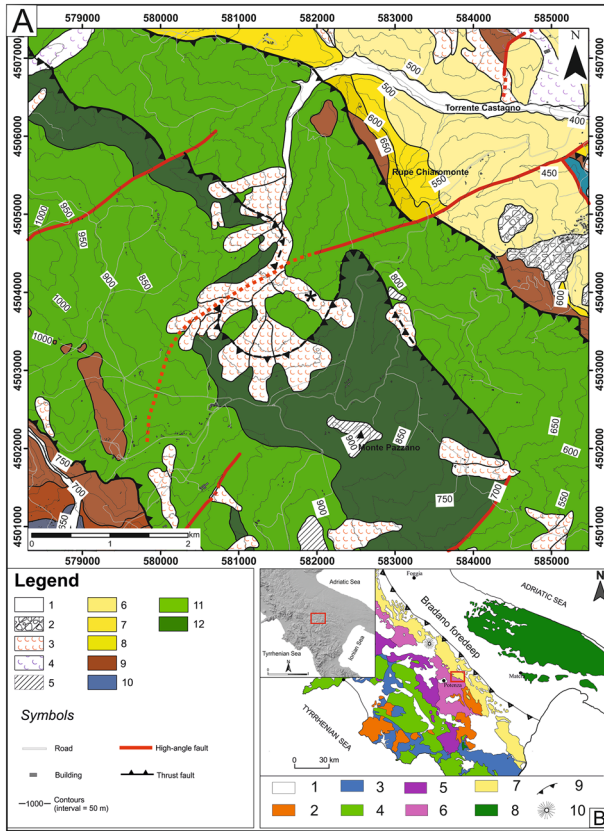


Fig. 1 **A** Geological outline of the study area: (1) alluvial deposits (Upper Pleistocene—Holocene); (2) slope deposits (Upper Pleistocene—Holocene); (3) landslide deposits (Holocene); (4) ancient landslide deposits (Upper Pleistocene—Holocene); (5) colluvial deposits (Upper Pleistocene—Holocene); (6) Grey-blue clay and silty clay (Sintema di Tolve, Lower–Upper Pliocene); (7) Massive sand and sandstone (Sintema di Tolve, Lower–Upper Pliocene); (8) Gravel and sandstone (Sintema di Tolve, Lower–Upper Pliocene); (9) Numidian sandstone (lower–middle Miocene); (10) Formazione di Corleto Perticara alternanza in strati di marne calcaree, calcari marnosi e calciliti (CPA); (10) calcilitites, marls and shales (Corleto Perticara Fm, Eocene—Oligocene); (11) Calcarenites and calcirudites with intercalation of marls and shales Flysch Rosso (Flysch Rosso Fm, upper Cretaceous—Oligocene); (12) Siliceous marls and shales (Galestri Fm, lower–middle Cretaceous). The black star indicates the studied landslide. **B** Geological sketch map of southern Italy (modified after Schiattarella et al. 2017). 1b. Pliocene to Quaternary units; 2b. Miocene siliciclastic units; 3b. Mesozoic–Cenozoic Internal units; 4b. Mesozoic–Cenozoic Apennine carbonate platform units; 5b. Mesozoic–Cenozoic Lagonegro basinal units; 6b. Mesozoic–Cenozoic Apulian carbonate platform units; 7b. Volcano; 8b. Thrust front of the chain

and gentler transport zone, and a lobate-shape toe. Discontinuous shear surfaces along the flanks of the lateral channels can be also recognized.

We have integrated traditional geomorphological analysis with DEM comparison and seismic surveys in order to: (i) study the multi-decadal spatial and temporal evolution of the landslide, (ii) estimate the volumes mobilized during the recent phases of slope reactivation; (iii) reconstruct the subsurface features of the landslide body and the geometry

of the sliding surface; (iv) infer the predisposing and triggering factors of the intermittent activity of the complex slow-moving landslide.

2 Methodology

Our analysis follows a workflow that integrates a detailed multitemporal landslide inventory with the interpretation of active and passive seismic surveys aimed at reconstructing the subsurface landslide features and bedrock depth (Fig. 2). Multi-temporal landslide inventory map has been prepared according to the methods, guidelines and suggestions of the wide scientific literature on the topic (see for example for a wide review Guzzetti et al. 2012; Soeters and van Westen CJ 1996). The geomorphological analysis was integrated with a quantitative volumetric analysis supported by the comparison of two UAV-derived DEMs (2020 and 2022). Such an approach allowed us to estimate the historical evolution of the complex landslide and the mobilized volumes in the depletion and accumulation sectors of the landslide.

To reconstruct the landslide geometry, geomorphological and topographic data were coupled with the following analyses: seismic refraction tomography (SRT), ambient noise measurements of the horizontal to vertical spectral ratio (HVSr) and multi-component, single-offset and multi-offset MASW. We test the reliability of such an integration between multisource and multiscale data for a fast, accurate and low-cost reconstruction of 3-D

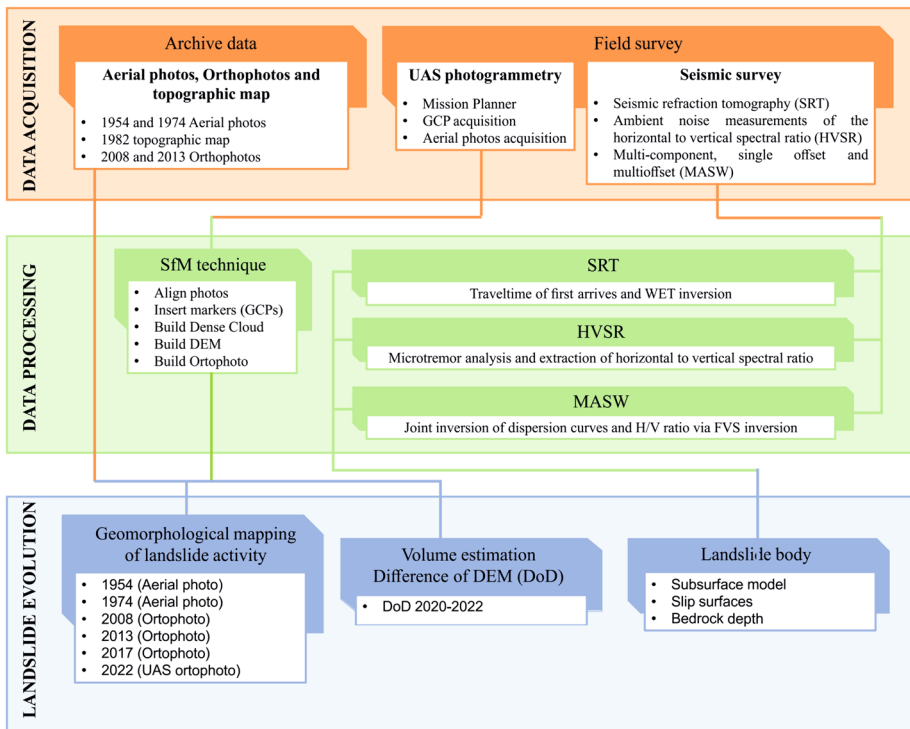


Fig. 2 Workflow of the acquisition and elaboration steps of the collected data

geometry of slow-moving complex landslides, especially for rural landslide areas where core drilling are not present.

2.1 Multitemporal geomorphological analysis

We use a variety of remote sensing data and methods to reconstruct the landslide dynamics during the period 1954–2022. The long-term analysis of the landslide evolution was performed by geomorphological interpretation of historical aerial photographs, satellite images, and UAV orthophotos.

A geomorphological analysis of the evolution of the Tolve landslide from 1954 to 2023 was carried out using a series of aerial photographs, topographic maps, and orthophotos. More specifically, a long-term analysis of the landslide evolution was carried out through the geomorphological interpretation of historical aerial-photos (years: 1954 and 1974), satellite orthophotos (years: 2008, 2013, and 2017), and UAV-based data (2020 and 2022).

Digital stereoscopic aerial photographs for 1954 and 1974 at scales between 1:15,000 and 1:33,000 were interpreted using the StereoPhotoMaker software. For each of the available photo pairs, the main landforms of the landslide were interpreted using well-established methods and procedures of geomorphological photo-interpretation (Guzzetti et al. 2012; van Westen and Lulie Getahun 2003; Conforti et al. 2014; Santangelo et al. 2015; Lazzari et al. 2018). The results were digitized in a GIS platform on ortho-rectified images and all the interpreted landforms include an attribute table with data on type and activity and uncertainty degree.

Adopting well-consolidated criteria of geomorphological photo-interpretation, relative age and activity of the complex landslide are inferred from the morphological characteristics and appearance on the historical aerial photos and orthophotos (Guzzetti et al. 2012 and references therein). On these basis, we adopt a classification scheme of the activity state of the landslide that follows the Italian Landslide Inventory (IFFI) project (Trigila et al. 2010). More specifically, the different sectors of the landslide are classified active if they appear fresh on the imagery of a given date. Dormant landslide sectors are sectors where morphological signs of possible re-activation exist whereas inactive ones include stabilized areas.

A synoptic geomorphological map and the landslide evolution pattern were then extracted for the following periods: 1954, 1974, 2008, 2013, 2017, 2020, and 2022.

For the years 2020 and 2022, topographic data and high-resolution DEMs (pixel size: 2 cm) were obtained through the elaboration of two drone surveys. Since land use is largely characterised by the absence of vegetation cover, we prefer to use photogrammetry instead of the LiDAR survey and exclude sectors with significant vegetation from the volume calculation. The surveys were carried out in May 2020 and August 2022. A DJI Matrice 210 with a 20 Mpx photogrammetric camera, a Trimble GNSS for ground target acquisition, and UgCS software for flight planning were used to collect photogrammetric data. Agisoft Metashape software was used to generate the 3D models. The software is based on the SfM algorithm (Fig. 2), which in input needs images and position of targets and in output releases a point cloud, orthophotos and DSM (James et al. 2019; Minervino Amodio et al. 2020).

During photogrammetric processing, the point cloud was not subjected to vegetation filtering because the study area is featured by the absence of vegetation, especially in the active area of the landslide. The UAV data allow us to reconstruct the short-term evolution of the landslide and also to make quantitative assessments of the mobilized landslide

volumes in the period 2020–2022. The volume involved in the Tolve landslide in the period 2020–2022 was derived from the difference of the DEMs (DoD) obtained during the SfM process. Small sectors of the study area with a significant vegetation cover was excluded by the DoD volume calculation. To obtain this result, the 'Volume Calculation Tool' within the QGIS software was used.

2.2 Seismic survey: background and applied methods

Active and passive seismic surveys are often used to reconstruct subsurface P- and S-wave velocity profiles, which can be easily correlated with the low-velocity layer associated to the thickness of the landslide bodies (Samyn et al. 2012; Capizzi and Martorana 2014; Imposa et al. 2017; Hussain 2019). Due to several limitations of seismic refraction tomographies (SRTs) (i.e.: low penetration depth, low reliability of the 2-D model in presence of a velocity inversion, low signal–noise ratio of seismograms, time-consuming acquisition workflow; see Dal Moro 2020; Hunter et al. 2022), many works dealing with landslide analysis have recommended the application of this method in combination with other techniques such as GPR and ERT (see e.g. Sass et al. 2008; Bekler et al. 2011; Imani et al. 2021; Himi et al. 2022) to infer the depth of the slip surfaces and to constrain the subsurface geometry of unstable slopes.

Recently, the application of surface wave (SW) methods, which record Rayleigh and Love Waves (Park et al. 1999; Dal Moro 2014), as well as the Horizontal-to-Vertical Spectral Ratio (HVSR, Nakamura 1989) have demonstrated their usefulness and effectiveness for the reconstruction of geometry of landslide slip surfaces and the subsurface geometry of mass movement processes (Irham et al. 2021; Widyadarsana and Hartantyo 2021; Alonso-Pandavenes et al. 2023; Wróbel et al. 2023 among others). Using a similar combined approach, we combine the interpretation of two seismic refraction tomographies (SRTs) with the analysis of dispersion curves of Rayleigh and Love waves and the horizontal-to-vertical spectral ratio (HVSR). On the basis of the large availability of correlation between lithotechnical features of landslide and bedrock deposits and P- and S-wave velocities (see for example Stucchi et al. 2013; Imani et al. 2021), we reconstruct the subsurface layers and the geometry of the landslide surfaces.

Common and standard techniques of SW analysis use multi-channel and multi-offset geophone arrays and the analysis are based on the picking of the fundamental mode on a dispersion curve, which shows the phase velocity as a function of the frequency (see for example Imposa et al. 2017). Such an approach is highly subjective and can provide poorly constrained and/or “wrong” shear-wave velocity profiles (Dal Moro et al. 2019; Dal Moro 2023). To overcome the subjective interpretation of the velocity-spectra (Dal Moro 2019b; Dal Moro 2023), we adopt an approach based on the joint inversion of multiple components (i.e.: the radial component of Rayleigh waves and Love waves) dispersion curves according to the Full Velocity Spectrum approach, a technique based on the computation of the misfit of the whole velocity spectrum without any interpretation of the observed velocity spectrum in terms of modal dispersion curves (see Dal Moro 2020 for more details on the background of the approach and its advantage than the conventional methods).

In addition, seismic refraction techniques and multi-offset MASWs typically require the use of an array of 24 geophones and long and complex acquisition procedures. Recently, there has been growing interest in approaches based on the use of a single multi-component geophone, which allows faster and more effective acquisition of multicomponent dispersion curves (Dal Moro 2019a; Dal Moro et al. 2019). These techniques require a single

triaxial geophone and simpler equipment, acquisition procedures, and field operations, which can be very effective for the investigation of large landslide areas with significant lateral variations in subsurface properties and challenging logistics. Velocity spectra can be jointly inverted with HVSR curves (Nakamura 1989; Arai and Tokimatsu 2005) to better constrain the velocity models, especially at deeper depths than those investigated by active seismic techniques.

In this work, we collected a comprehensive seismic dataset including SRTs, multi-component surface-wave analysis, and HVSR along the whole landslide area with the aim of a robust characterization of S-waves velocity models. Figure 3 shows the location of the seismic surveys while Table 1 summarized the type of surveys, field equipment and acquisition procedures.

2.3 SRT

SRT records the arrival times (“first breaks”) of compressional and shear waves on a set of geophones, which allow to reconstruct a model of the P wave distribution in the subsurface. Such data are interpreted in terms of variations in the elastic properties of the subsurface by an iterative inversion of the travel time of surface waves derived from a manual picking of first arrivals. In this work, we have used the Rayfract software and the Wavepath Eikonal Traveltime (WET) inversion method. Lateral measurements of surface-wave velocity profiles can then be collated to produce 2-D sections of interpolated P-wave velocity. Two nearly orthogonal SRT surveys were carried out in the upper sector of the active earthflow (see Table 1 for more details about the configuration and acquisition procedures).

2.4 Surface wave analysis

Two multi-component and multi-offset MASW were acquired along the same arrays of the seismic refractions. The seismic acquisition was performed by placing a set of 24 geophones at different offsets (Table 1). To avoid the problems of ambiguous and non-unique solutions of the subsurface wave-velocity models derived by interpreting the vertical component of Rayleigh waves (Dal Moro 2023), we perform a multicomponent analysis of the surface waves by the acquisition and joint analysis of Love waves and the radial component of Rayleigh waves. Moreover, we applied the FVS approach, and a joint inversion was performed by using phase velocity spectra of the two components and the HVSR curve (see Dal Moro and Ferigo 2011; Dal Moro 2019b for a wider description of the methodological approaches and Dal Moro 2023 for a detailed review of limitations and advantages of the different methods of surface wave analysis). Such an analysis was performed by using the Winmasw Academy 2019 software and allowed us to strongly reduce the uncertainty of the S-wave velocity models. Such an active technique requires only one 3-component geophone at a one single-offset, which is used to estimate the group-velocity spectra of three “objects” (component of Rayleigh waves or Z component, radial component of Rayleigh waves or R, transversal Love waves or T component, see Dal Moro 2019a). Group velocities can be jointly inverted with the H/V curve acquired with the same triaxial geophone. We exploited this advantage of a simpler field procedures than the “standard” analysis of the multi-offset data by acquiring five single-offset multicomponent MASW to better define the subsurface features of several sectors of the landslide where it is logistically complicated to acquire multi-offset data.

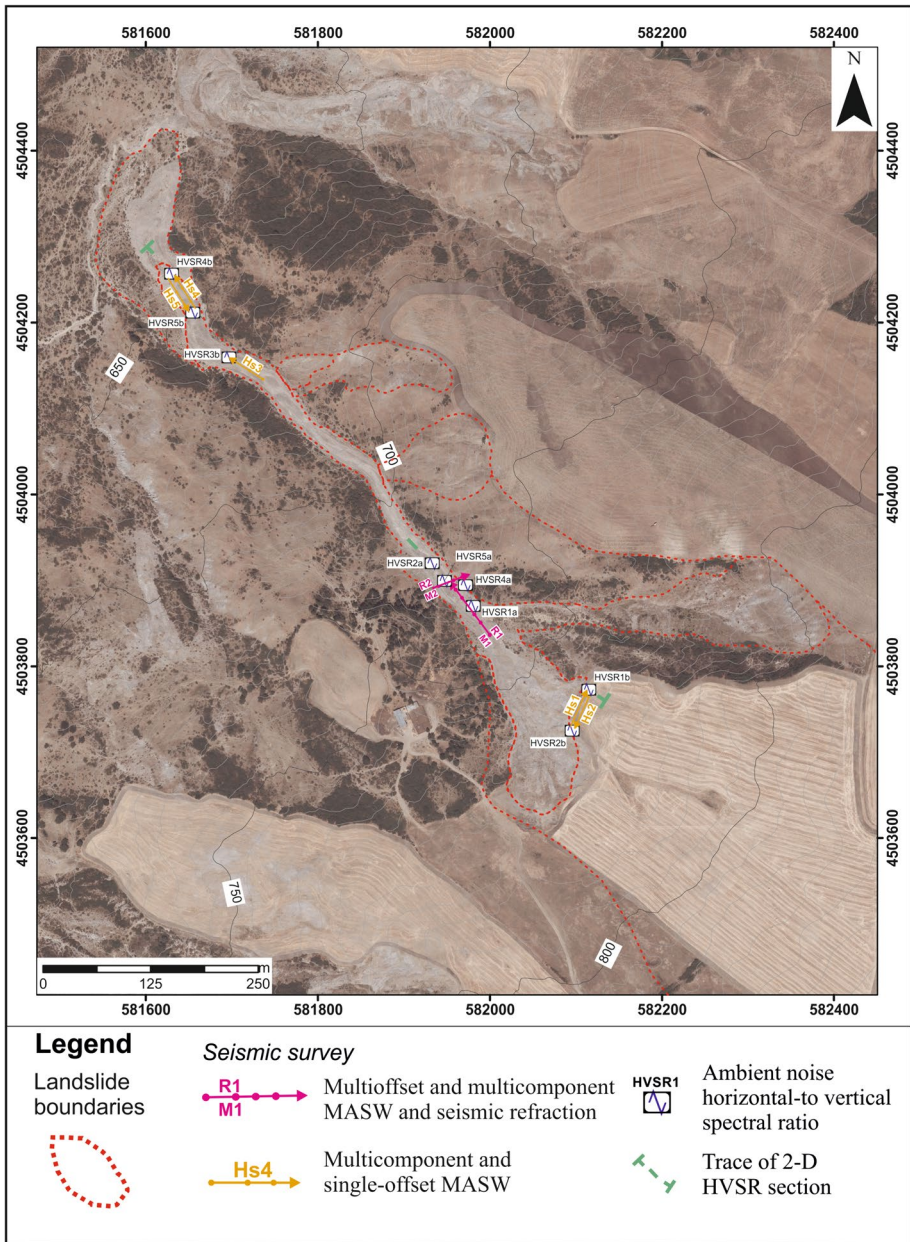


Fig. 3 Orthophoto (year: 2017) of the Tolve landslide with the location of the seismic surveys

2.5 HVSR

We also record seven passive datasets of ambient noise measurements to determine the HVSR curve (Nakamura 1989). We use the same single 3C geophone used for the

Table 1 Main acquisition parameters and detail about the array geometry and equipment of the seismic surveys

Seismic refraction tomography (SRT)								
Name	Measured parameter	Geophone type	Number of channels	Source type	Geophone distance	Array Length	Offset of external shots	Number of shots
R1	P wave velocity	Vertical—4.5 Hz	24	Hammer—Vertical	3 m	75 m	3 m	8
R2	P wave velocity	Vertical—4.5 Hz	24	Hammer—Vertical	2 m	48 m	0.5 m	8
Multioffset and multicomponent MASW								
Name	Measured parameter	Geophone type	Number of channels	Source type	Geophone distance	Array Length	Minimum offset	Number of shots/Stack
M1-ZVF	Vertical component of Rayleigh wave	Vertical—4.5 Hz	24	Hammer—Vertical impact	3 m	72 m	3	15
M1-RVF	Radial component of Rayleigh wave	Horizontal—4.5 Hz	12	Shear source—Hammer and horizontal plate	6 m	72 m	3	15
M1-THF	Love wave -THF	Horizontal—4.5 Hz	12	Shear source Hammer and horizontal plate	6 m	72 m	3	15
M2-ZVF	Vertical component of Rayleigh wave	Vertical—4.5 Hz	24	Hammer—Vertical and	2 m	46 m	0.5 m	12
M2-RVF	Radial component of Rayleigh wave	Horizontal—4.5 Hz	12	Shear source Hammer and horizontal plate	4 m	72 m	0.5 m	12
M2-THF	Love wave -THF	Horizontal (perpendicular to source)—4.5 Hz	12	Shear source Hammer and horizontal plate	4 m	48	0.5 m	12
Single offset and multicomponent MASW								
Name	Measured parameter	Geophone type	Number of channels	Source type	Source-geophone distance	Array Length	Minimum offset	Number of shots/Stack
HS1	Vertical and radial component of Rayleigh wave, Love wave	Three-component geophone—4.5 Hz	3	Hammer—Vertical impact and shear source	48 m	48 m	48 m	20

Table 1 (continued)

Single offset and multicomponent MASW

Name	Measured parameter	Geophone type	Number of channels	Source type	Source-geophone distance	Number of shots/Stack
HS2	Vertical and radial component of Rayleigh wave, Love wave	Three-component geophone	4.5 Hz 3	Hammer—Vertical impact and shear source	48 m	15
HS3	Vertical and radial component of Rayleigh wave, Love wave	Three-component geophone	4.5 Hz 3	Hammer—Vertical impact and shear source	38 m	15
HS4	Vertical and radial component of Rayleigh wave, Love wave	Three-component geophone	4.5 Hz 3	Hammer—Vertical impact and shear source	47 m	18
HS5	Vertical and radial component of Rayleigh wave, Love wave	Three-component geophone	4.5 Hz 3	Hammer—Vertical impact and shear source	47 m	15

acquisition of active single-offset acquisition. Records were made according to the guidelines and procedures proposed by the Sesame project. Fourier spectra of the north–south, east–west, and vertical components are calculated. The spectra of the horizontal and vertical components are then compared to estimate the H/V ratio as a function of frequency.

3 Regional and local setting

The landslide developed along a NW–SE-trending slope in the headwater sectors of a small drainage basin of the frontal sector of the southern Apennines. The catchment extends along the right-side of the Torrente Castagno river, a low-hierarchical order tributary of the Bradano River. This sector of the chain (Fig. 1) is characterized by NW–SE-trending morpho-structural ridges and thrust sheets, mainly moulded into Cenozoic sandstones, marls, and clays forming the eastern imbricate fan of the orogenic wedge (Riviello et al. 1997; Pescatore et al. 1999). These deposits show a high degree of deformation and are tectonically overlapped on Pliocene clastic deposits of thrust-top basins (Riviello et al. 1997). Pliocene deposits mainly characterize the easternmost sectors of the study area and are represented by a thick succession of transitional to marine environment consisting of conglomerate, sandstone and grey silty clays.

In this sector of the outer belt of the chain, the landscape is affected by widespread landslide phenomena and exhibits a gentle topography as a result of the diffuse outcrop of clay-rich tectonic units (Schiattarella et al. 2017; Lazzari et al. 2018). Steeper slopes and higher-relief sectors are preferentially distributed on NW–SE alignments of Numidian sandstones and coarser-grained Pliocene deposits. Mass movement processes are mainly associated with large-scale earthflows and widespread shallow landslides, which show a spatial distribution strongly influenced by the litho-structural setting and degree of tectonic deformation (Lazzari and Gioia 2016; Lazzari et al. 2018; Spalluto et al. 2021; Ardizzone et al. 2023).

This diffusion of large and deep-seated landslide processes promoted the local occurrence of landslide-dominated landscapes, which mainly affected catchments featured by wider outcrops of clay-rich highly deformed tectonic units such as Flysch Rosso and Argille Varicolori Fms (Borgomeo et al. 2014; Cotecchia et al. 2015; Lazzari et al. 2018; Ardizzone et al. 2023). The most impressive mass movements are complex landslides (*sensu* Cruden and Varnes 1996), which usually started as rotational slides in the calcareous-bearing lithologies, and evolved into flows in the lower sectors. Flows of fine-grained material occurred in narrow and elongated U-shaped or concave valleys and mobilized landslide deposits can move slowly for hundreds of meters before expanding in the lower relief areas (the *thalweg* of the main river). Several historical and geomorphological evidences suggest that these landslides have a multi-millennial evolutionary history and probably developed during the cold periods of the Late Pleistocene (Bertolini et al. 2017). Moreover, they often have a spatial distribution that appears to be controlled by the presence of regional tectonic lineaments.

The Tolve landslide cut a slope with a main SE–NW orientation located on the right side of the headwater sectors of the Torrente Castagno catchment (Fig. 3). This sector is dominated by several large landslides, which developed as rotational slides in their upper sectors and evolves as earthflows in the lower altitude areas. At a larger scale, these huge landslides form an arcuate depletion zone with a diameter of 6 km and their accumulation zones converge radially in the main valley of the Torrente Castagno river (Fig. 1). The middle and lower sectors of the unstable slope are mainly carved in Lower–middle Cretaceous

siliceous marls and shales of the Flysch Rosso Formation. In the higher altitude sectors of the study area, light-grey and greenish shale with intercalation of thin beds of marls and marly limestone (Galestri Fm., Lower-Middle Cretaceous, Fig. 1) crop out. They overlay tectonically clay-rich deposits of the Flysch Rosso Formation. The Tolve landslide (Fig. 4) is about 1300 m long, has a total relief of 215 m, and covers an area of about 270,000 m². The average slope of the landslide is about 21°, with steeper and higher-relief landforms located in the upper sectors and a gentler topographic pattern in the central and lower ones.

The climatic setting of the study area shows a Mediterranean-type annual and seasonal distribution of precipitation. The rainfall recorded at the stations of Vaglio di Basilicata and Oppido Lucano over the last 50 years shows an average annual value of total precipitation of about 600 mm, with a strong seasonal variability and a predominant concentration of rainfall in autumn and spring. During these seasons, multi-days heavy rainfall events associated with peaks of 2 or 3 days of severe precipitation have been observed. The recent trend (i.e.: in the last 20 years) of rainfall data suggests a general decrease or stability in total annual rainfall and an increase in both dry periods and maxima in multi-day rainfall events.

4 Results

4.1 Geomorphological analysis and multitemporal activity maps

The landslide head scarp (Fig. 4) is located at an elevation of about 825–835 m and the arcuate source area shows peculiar geomorphological evidences such as widespread surficial erosional features, counterslopes, and hummocky-type topography. They suggest a movement of the depleted mass with a roto-translational geometry, which mainly affected the calcareous-rich deposits of the Galestri Fm. Downslope, the source area fed a narrow flow channel (i.e.: width of about 25–30 m) composed of heterogeneous and unconsolidated fine-grained material developing in a valley with an average slope of about 11–12°. The narrow valley is laterally bounded by channels separating the flowing material from the undeformed material. The main valley was also fed by several secondary lateral shallow landslides in the deposits belonging to the Flysch Rosso Fm. The landslide toe expands at an altitude of 640 m, forming a fan-shaped foot that ends in the Torrente Castagno river. The toe is partially incised by the main river.

Visual inspection of the 1870 IGMI map and in particular the contour pattern shows that the main elements of the complex landslide are already present in the slope. As highlighted by radiocarbon dating of similar landslides in the Apennines (Bertolini et al. 2017; Leonelli and Chelli 2024) and other geomorphological evidences (Aringoli et al 2013; Di Maio et al. 2018), this could suggest that the initial failure of the large-scale landslide has a multi-millennial age and can likely relate to the Late Pleistocene periglacial conditions. The recent geomorphological evolution of the unstable slope is mainly related to a partial reactivation of the landslide body, especially in its middle and lower part. The present-day active landslide occurs at altitudes ranging between 780 and 635 m a.s.l., as a result of a partial re-activation of the pre-existing ancient landslide. The active landslide shows geomorphological features typical of an earthflow such as a circular and steep scarp, a narrow transport zone, and a fan-shape toe.

Geomorphological analysis of the 1954 stereo-pairs (Fig. 4) highlights that the main elements of the complex landslide are already developed. A wide arcuate source area with

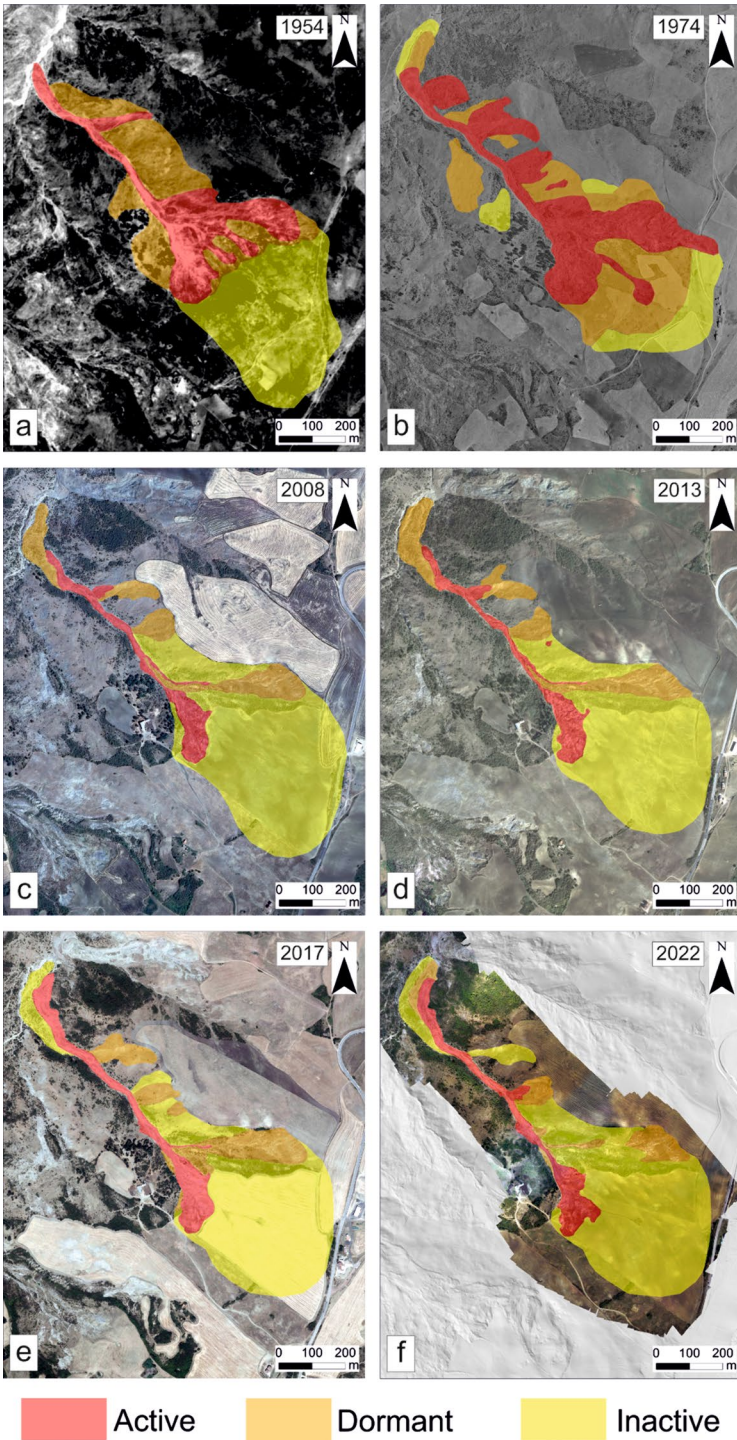


Fig. 4 Multitemporal landslide activity maps of the study area

limited evidence of activity was observed at higher elevations while the active sector of the landslide is located in the middle sector of the slope. The most significant increase in the active sectors of the landslide can be observed on the 1974 aerial photographs. The geomorphological analysis shows a significant retrogression in the north-eastern and central sectors of the slope and an advancement of the toe. Widespread shallow landslides are active along the left flank of the earthflow. Multitemporal landslide maps of the study area highlight a general decrease of the active sectors of the landslide from 1974 to 2022 (Fig. 4). Between 2013 and 2020, the active source area of the earthflow extended upslope of about 30 m while the toe advanced of about 90 m. Localized smaller movements can be detected in recent years.

4.2 Seismic survey and subsurface characterization of the landslide

4.2.1 SRTs

R1 SRT (Fig. 5) deriving by inversion of first-arrival traveltimes highlights the presence of a shallower layer characterized by a low P-wave velocity of $300\text{--}500\text{ m}\cdot\text{s}^{-1}$. The low P-wave velocity layer has a thickness of about 2–3 m and can be correlated with the presence of unconsolidated sediments and reworked blocks with surficial cracks, voids, and fracture zones. At a depth of about 5–7 m, a well-defined refractor can be recognized (see the wavepath coverage in Fig. 5a). It can be roughly located along the $1500\text{--}1600\text{ m}\cdot\text{s}^{-1}$ isolines and probably corresponds to the saturated part of the active slip surface. Deeper layers are characterized by higher values of P-wave velocity.

R2 SRT (Fig. 5b) shows a spatial distribution of P-wave isolines quite similar to the R1 SRT. The surficial low-velocity layer has a depth ranging from 0,5 to 2 m, a concave geometry, and a maximum depth in the central sector of the array. The main refractor can be observed at a depth of 5–7 m.

4.2.2 HVSR

All HVSR curves (Fig. 6) show a maximum with an amplitude value ranging between 1.5 and 3.5 at a relatively high frequency (i.e.: between 4.5 and 15 Hz, Fig. 6a), which can be interpreted as related to a significant surficial discontinuity in the V_s profile. The V_s contrast can be correlated to the abrupt increase in V_s values between the active landslide body and the lower “undeformed” layers. The main peak in the H/V curves tends to move towards lower frequencies from HVSR1a (Inline position 1 in Fig. 6b) to HVSR4b (inline position 7 in Fig. 6b). Such a trend suggests a variation (i.e.: an increase) along the slope of the depth of the shallower lithological discontinuity (i.e. Fig. 6b depicts such geometry of the active sliding surface across the whole landslide).

4.2.3 SW analysis

Multi-component MASWs were acquired over the whole area of the active earthflow (see Fig. 3 for the location of the seismic data). Figure 7 illustrates the seismic dataset and the relative joint inversion for the M1 multi-offset and multi-component MASW: the joint inversion between the group velocities of the R and T components (offset: 57 m, Fig. 7) and the HVSR curve shows a V_s model with a solution that well-fitted the collected data.

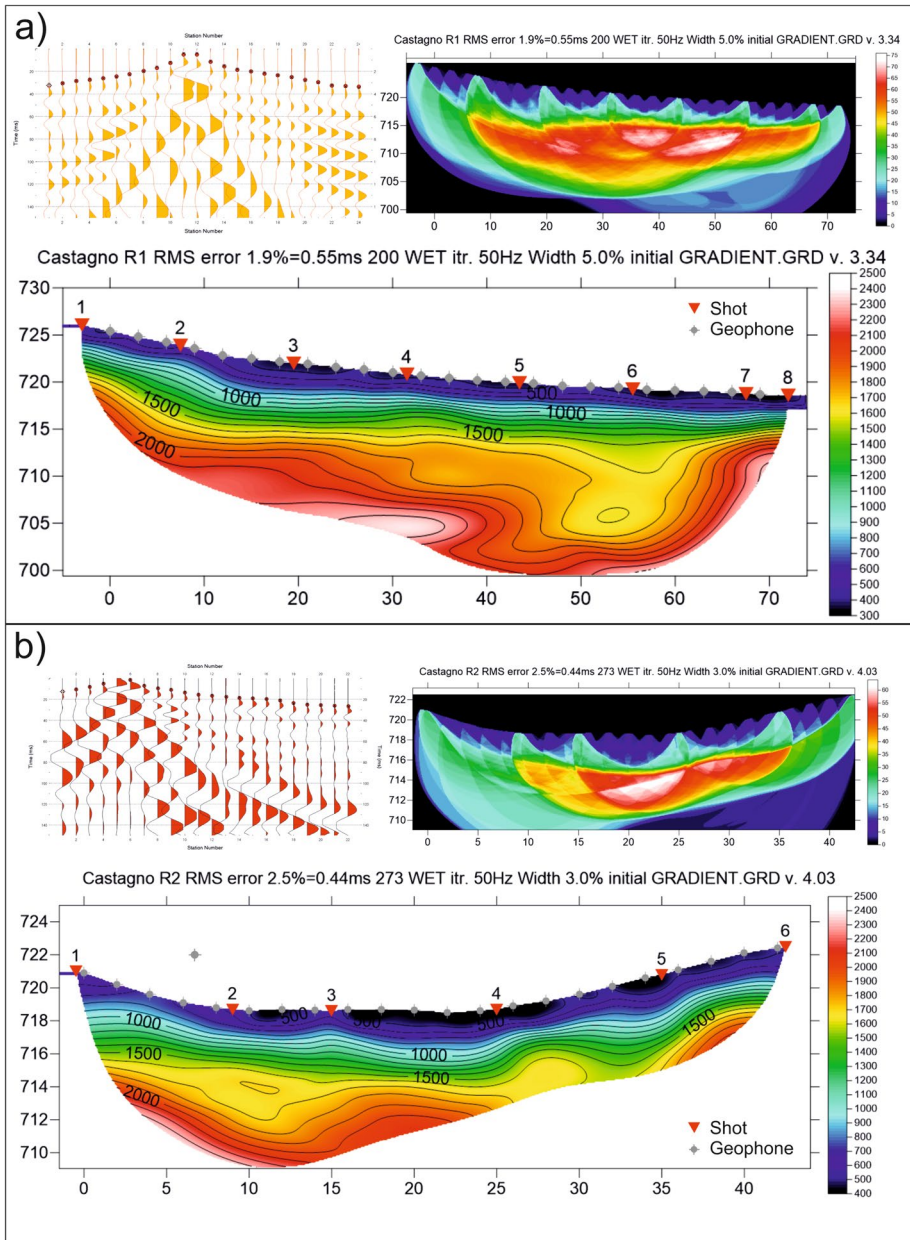


Fig. 5 Results of the P-wave seismic refraction survey. **a** Example of picking (to the left) of a refraction seismic shot recorded during the SRT1 acquisition, wavepath coverage (right) and inverted seismic refraction tomography (bottom). **b** Picking (left) of a refraction seismic shot relative to the SRT2 acquisition, wavepath coverage (right) and inverted seismic refraction tomography (to the bottom)

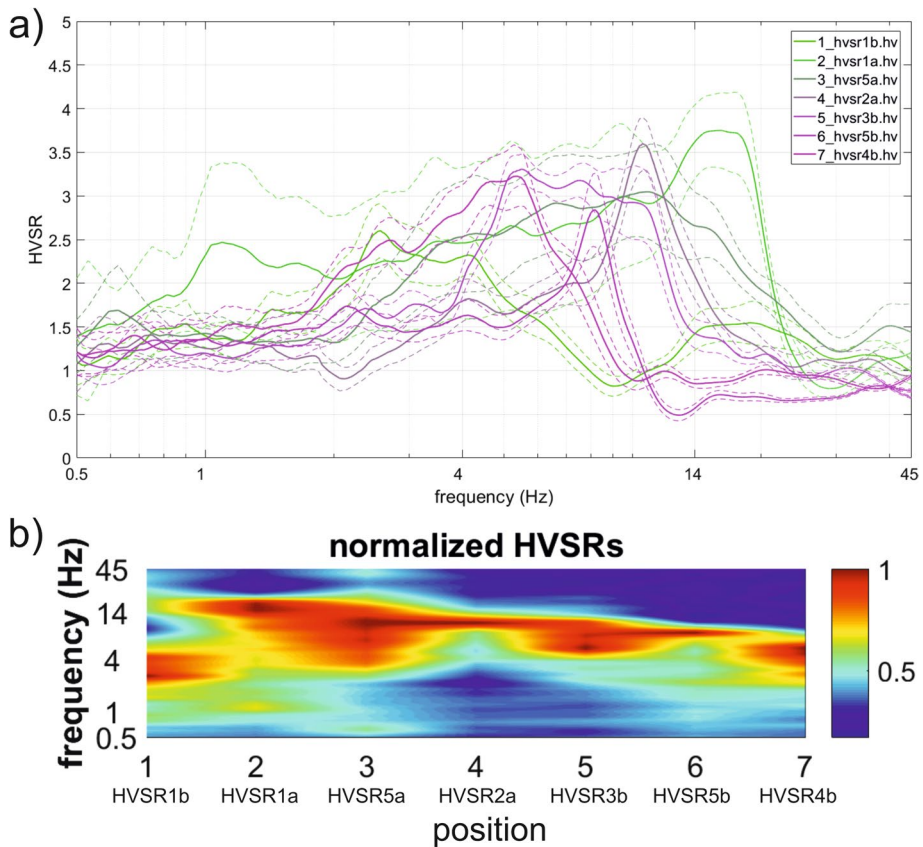


Fig. 6 HVSR curves (a) and 2-D HVSR section (b, trace in Fig. 3) of the study area. The 2-D section was constructed by a normalization of the maximum value of the H/V amplitudes. Note the progressive shift of the main H/V normalized peak

Apart from the visual good fitting between the field datasets and the best theoretical models, the robustness of the joint inversion and, in general, of the reconstructed V_s profiles was confirmed by low values of the misfit between reconstructed and acquired datasets. The S-wave profile is featured by a low-velocity layer (i.e.: V_s value of about 150 m/s) with a thickness of about 4 m, which passes downward to a layer with a V_s value of 240 m/s. At a depth of 11.5 m, the velocity model shows an increase in values from 240 m/s to 320 m/s. Deeper layers highlighted V_s value higher than 400 m/s.

The seismic data acquired at different locations across the active landslide areas are grouped into three sectors (Fig. 8): the upper sector or source area (HS1 and HS2), the middle sector or transition zone (M1 and M2), and the landslide toe (HS3, HS4, and HS5). Comparison of the V_s profiles obtained for the other sites indicates a substantial homogeneity of the reconstructed seismic features (Fig. 8). In fact, the surficial low-velocity layer can be recognized in all the V_s profiles derived from the interpretation of the multi-component MASWs (layer 1 in Fig. 8). V_s value lower than 150 m/s can be attributed to unconsolidated deposits and can be correlated with the thickness of the active landslide body. Intermediate V_s values with a high variability (i.e.: from about 250 to 450 m/s) were

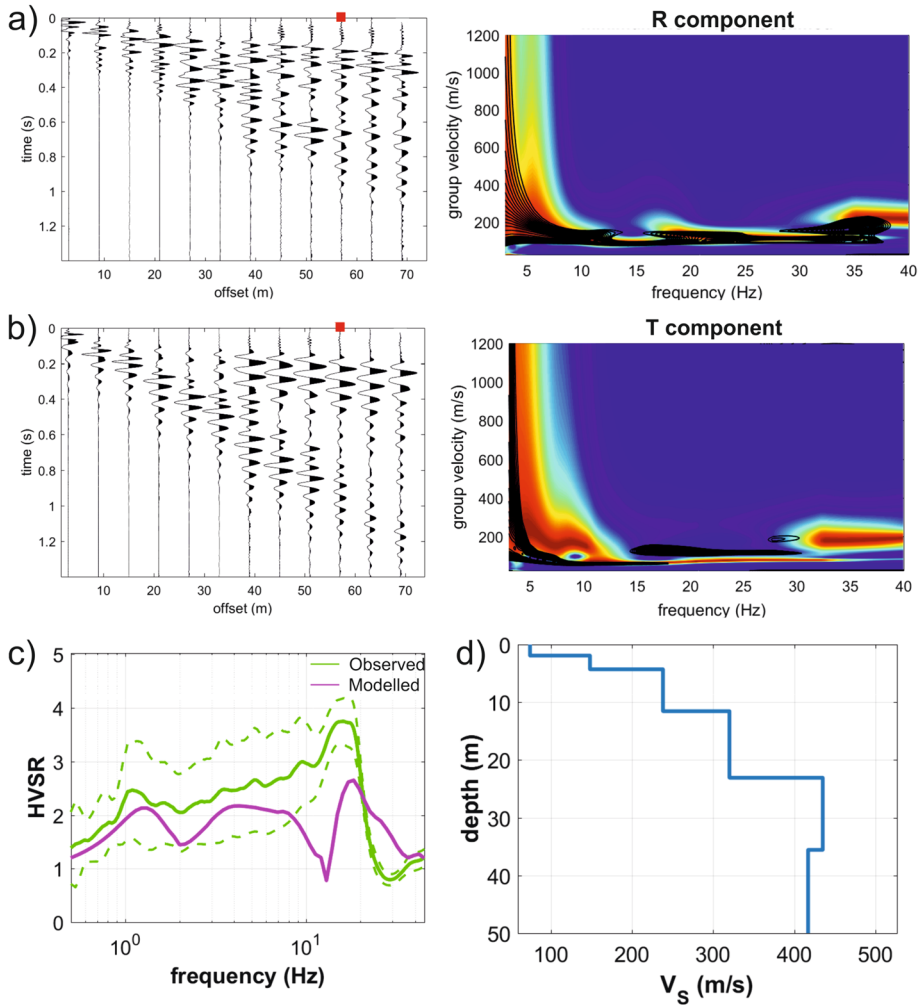
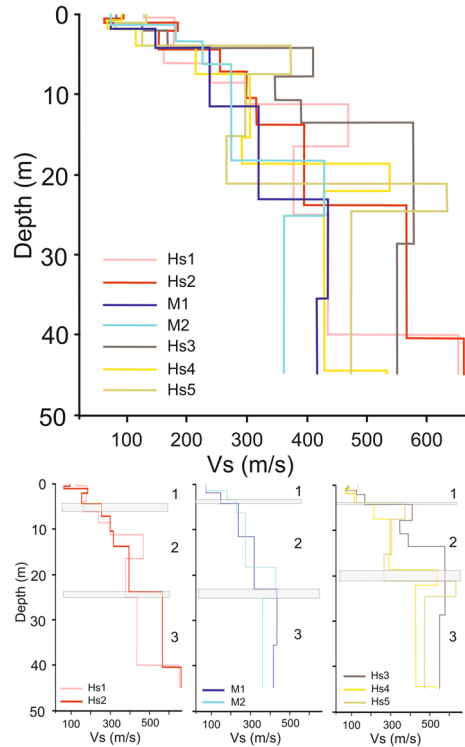


Fig. 7 Analysis of the multi-component and multi-offset MASW M1 (see Fig. 3 for location): **a** seismic traces and group-velocity spectra (trace 10, offset 57 m) for the radial (R) component of Rayleigh waves; **b** seismic traces and group spectra of the transversal Love waves. Black contour lines represent the synthetic group spectra of the best model derived by joint inversion; **c** observed HVSR and synthetic curve of the best model; **d** V_s profile derived from the joint inversion of group velocity spectra and HVSR curve. The group velocities of the Z and R components were inverted according to the Full Velocity Spectrum (FVS) approach (thus avoiding the spectra interpretation in terms of modal curves) and the best model is also reconstructed by a joint inversion of dispersion curves and HVSR curve

observed at depths ranging from 4 to 25 m. Such a variability is more pronounced in the source and accumulation areas of the active earthflow (Fig. 8b and d). These layers can be roughly correlated to the thickness of deposits involved in slope failure phenomena (layer 2 in Fig. 8). The V_s profiles reached the considerable value of about 500 m/s at depths higher than 18–25 m. The abrupt transition between a layer with intermediate S-wave velocities and the highest velocity layer can be a robust indication of the presence of stable bedrock.

Fig. 8 Synoptic scheme of the Vs profiles derived by multi-component MASWs and relative interpretation in terms of the subsurface features of the studied landslide (see text for additional details)



The variability of the Vs values in the deeper layers can be related to the presence of the alternation of clay-rich deposits and stiff (i.e. calcareous) layers.

4.3 UAS survey and short-term landslide evolution

Short-term evolution of the slow-moving Tolve landslide was performed by a visual and quantitative analysis of DEMs derived from the two UAV surveys (year 2020 and 2022). The vertical errors of the two DEMs with respect to GCPs in photogrammetry modeling are distributed around a value of about 3 cm. Figure 9 depicts the change in surface elevation related to the movements from November 2020 to August 2022. Along the entire main body of the landslide the DoD shows a gradual transition of material loss in the upper and mid-high parts to accumulation in the lower part with colours tending towards the red. The movement of material along the slope can also be seen along the topographic profiles between the two DEMs. The DEM of difference (DoD, Fig. 9) highlights a clear decrease in topography (up to 3 m) in the landslide source area. In Fig. 9a, topographic profiles drawn for DEM 2020 (red line) and DEM 2022 (yellow line). Such a topographic modification suggests a recent reactivation of the earthflow with a retrogressive trend.

The upper sector of the transport zone is mainly characterized by an increase of the topographic surface, which can be roughly related to the accumulation zones of the recent landslide movements. In the lower sector of the transport zone, the altitude comparison shows limited topographic variation with localized topographic modification

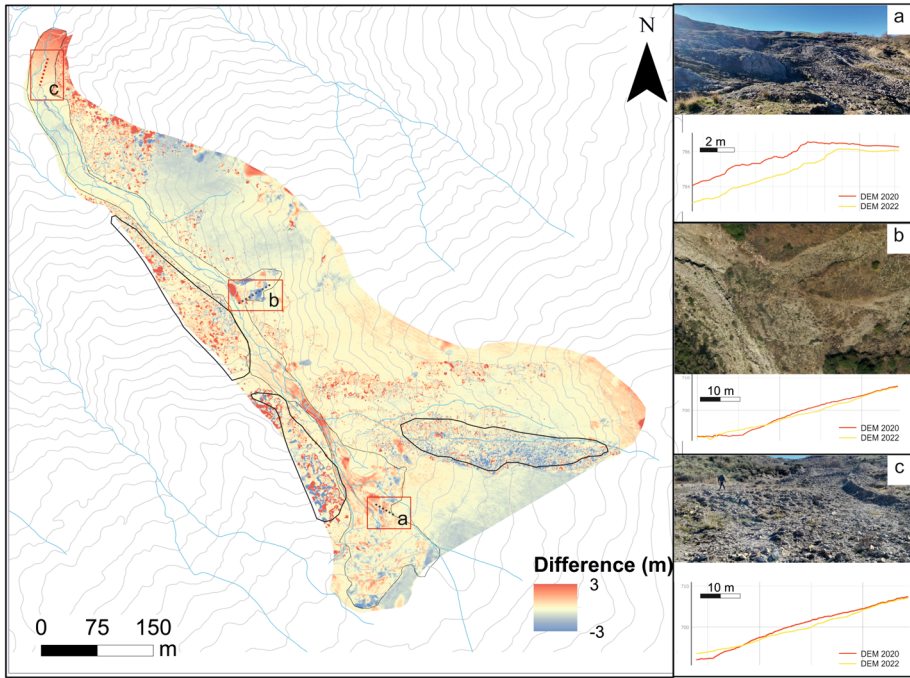


Fig. 9 Elevation difference map between May 2020 and August 2022 of the Tolve landslide. The black polygons indicate areas characterised by the presence of vegetation; these areas were not taken into account for the calculation of the topographic modification. A polygon with a thin line in black shows the active landslide area as of 2022

due to lateral shallow landslides (see for example the frame b in Fig. 9). Significant topographic variation occurred at the toe of the active landslide, where our analysis detects an increase of the elevation between 2 and 3 m (Fig. 9c). The landslide volume variation was quantified to be approximately -993.6 m^3 , with an accumulated volume of 1646 m^3 and a depleted value of 2640.6 m^3 (with an estimated error of 10.4%). The DoD (Fig. 9) shows a general trend characterised by loss in the upper part of the landslide and accumulation in the lower part. The missing volume is probably due to the material that accumulated and came out of the UAV-surveyed area.

5 Discussion

The landscape of the southern Apennine chain is largely affected by widespread landslide phenomena of different size, type and kinematics, especially in its outer/frontal belt due to the combination of different predisposing factors such as high relief, outcrops of highly-tectonized and clay-rich, deposits, and presence of tectonic lineaments. In particular, large earthflows are a common landform in southern Italy and their recent re-activation has frequently represented a severe factor of risk for socio-economic activities, infrastructures, and settlements (Giordan et al. 2013; Cotecchia et al. 2015; Spalluto et al. 2021; Ardizzone

et al. 2023). Therefore, a detailed and comprehensive investigation of the spatio-temporal evolution and geometry of these landslides as well as an assessment of the possible triggering factors capable of mobilizing their different sectors is crucial for purposes of regional hazard assessment and mitigation planning.

We investigated the long-term evolution of the Tolve landslide, a complex slow-moving landslide located in one of the most impressive landslide-dominated landscapes of the Basilicata region by integrating traditional geomorphological analysis, UAV-based monitoring, and seismic surveys.

Our approach has allowed us to define the multi-decadal spatial evolution of the slope and to estimate the volumes mobilized during the most recent stages of the landslide evolution. This multi-source, multi-disciplinary approach, which includes geomatic techniques and the comparison of high-resolution DEMs, has been useful in highlighting how different sectors of the unstable slope can be reactivated following major rainfall events. This is probably due to the climatic setting of recent years, which does not change so much in the total amount of rainfall but is characterised by extreme events concentrated in a few hours (see Fig. 11).

The application of different seismic techniques has been particularly useful in defining the thickness of the present-day active landslide body and the geometry of the deeper and older sliding surface. SRT is one of the more consolidated geophysical methods for the 2-D characterization of landslide boundaries, depth of sliding surfaces, and saturated layers. Its main limitations are related to a significant field effort, a difficulty to generate seismograms with a good signal to noise ratio, and a low penetration depth. In this work, we have encountered all the above-mentioned issues. In addition, the extensive use of the seismic refraction method for the characterization of large and hardly-accessible unstable slopes such as the study area is really unsuitable. For these reasons, we have exploited the great potential of single-offset multicomponent MASW as an effective and valuable tool for defining the subsurface features of large landslides with a low accessibility. Due to the simplicity of the equipment (i.e.: a single triaxial geophone) and the rapid and easy acquisition procedures, such an approach can represent a novel and robust technique to extract information about the 2-D geometry of large and deep-seated landslides.

The studied landslide extends for a total length of approximately 1300 m and exhibits typical features of a slow-moving landslide with a long-term evolution of intermittent activity. According to the oldest available topographic map of the study area, the initial slope failure occurred before the second half of the nineteenth century. It developed as a rotational slide in the higher-altitude sectors and evolved into an earthflow in the lower ones with a maximum depth of the initial slip surface events of about 20–25 m (Fig. 10). The spatial and temporal evolution of a multi-stage complex landslide located in a catchment of the frontal sector of the southern Apennine chain was reconstructed by multitemporal geomorphological analysis, near-surface seismic survey, and DEM comparison. The Tolve landslide shows a multi-decadal evolution characterized by intermittent periods of activity and dormancy. Geomorphological evidences suggest that the initial failure of the large-scale landslide has a multi-millennial age and can be related to a roto-translational movement that evolved in an earthflow. Recent evolution is associated with a major reactivation event in the middle and lower sectors of the larger complex landslide, which probably is related to a heavy rainfall event occurred in January 1972. Recent evolution is mainly associated with minor movements in the source area, toe advancements, and widespread shallow landslides along the flank of the earthflow. A significant increase in the landslide activity was reconstructed by analyzing the 1974 aerial-photographs.

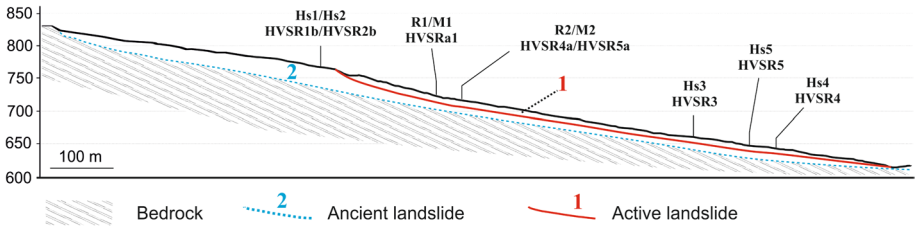


Fig. 10 2-D Section of the Tolve landslide with the reconstruction of the slip surfaces as inferred by seismic data

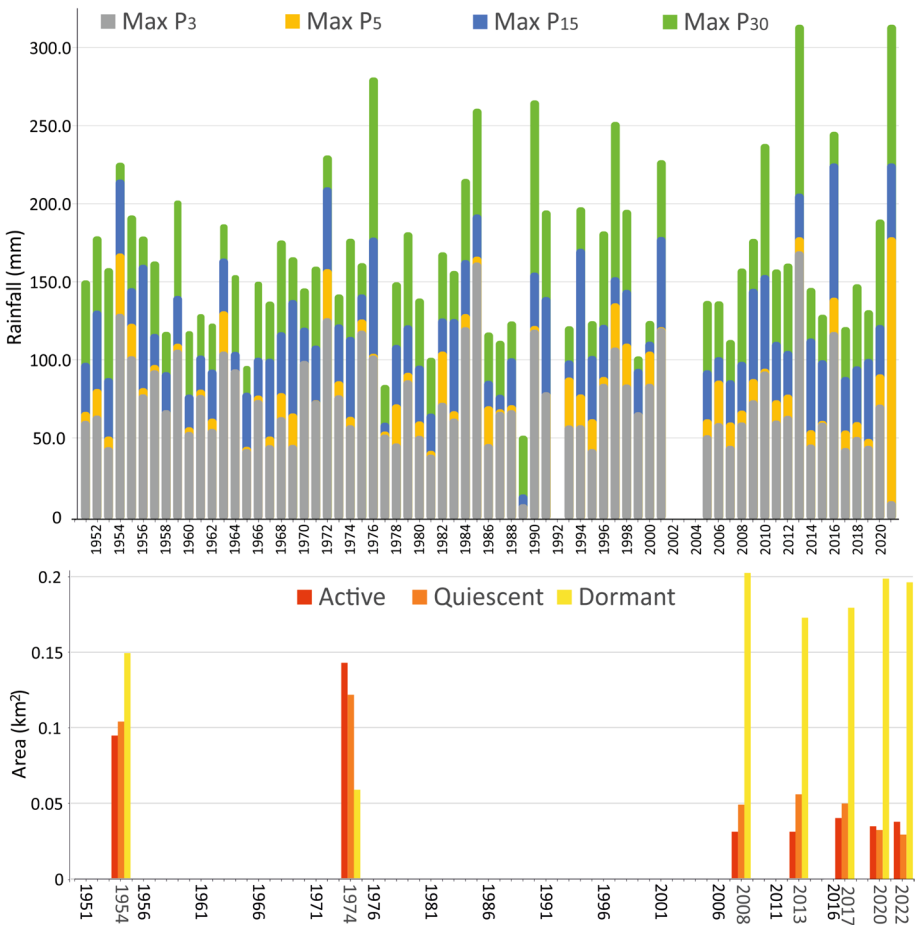


Fig. 11 Graph of temporal trend of activity and relationships with rainfall data. MaxP3, MaxP5, MaxP15, and MaxP30 are the annual maximum of cumulative rainfall data for 3, 5, 15 and 30 days

We reconstructed a significant retrogression of the depletion zone with a multiple upslope migration of crown areas in the north-eastern and central sectors and the highest value of active landslide areas (Fig. 11). The re-activation of pre-existing and deeper complex landslides of probable post-glacial age has often been reconstructed as a typical geomorphic response of unstable slopes with similar characteristics to the study area (Pánek 2014; Bertolini et al. 2017). Between 16 and 23 January, precipitation reached a significant value of 155 mm. On 25 January, an additional 40 mm of rain fell. Such an event represents one of the heavy rainfall events of the available climate record. The re-activation of the landslide observed in 1974 stereo-pairs can be likely correlated to that period of heavy rainfall occurred in January 1972 (Fig. 11).

Seismic data and in particular the distribution of the V_s values in the surficial layers suggest that the movement of the active earthflow occurred within a deformation zone with a limited thickness of about 3–4 m. Moreover, SRTs indicate a depth of about 5–6 m of the saturated layer. It has been widely demonstrated that slow-moving landslides and earthflows show geomorphic evidence of movement/activity during a relatively long period of high precipitation. Such heavy rainfall events can promote water infiltration, water-table raise, and local saturation of the fissured near-surface material (Lacroix et al. 2020).

Younger geomorphological evolution of the studied slope is characterized by a general decrease of the active sectors of the landslide and smaller topographic modification in the source area and accumulation zone of the earthflow (Fig. 9). Although the analysis of historical rainfall record highlights the occurrence of heavy rainfall events with features similar to those of 1972, our geomorphological analysis suggests that these events are not able to promote a significant mobilization of the earthflow and limited recent (i.e. in the latest 10 years) movements are intermittent and localized in the intermediate sectors of the investigated slope. Such an evidence could be explained by considering the general slope reduction induced by the main (i.e.: January 1972) reactivation or the reduced ability of the main river to erode the landslide toe.

6 Concluding remarks

Impressive and large-scale slow-moving landslides with a long-term evolutionary history of activity and dormancy are a common landform in the mountain belt of the southern Apennines. The comprehensive study of the Tolve complex landslide was carried out by integrating detailed multitemporal mapping of the landslide activity with the reconstruction of subsurface landslide features based on active and passive seismic data. Geomorphological analysis and landslide activity map indicate that the Tolve landslide has a multi-millennial age and can be classified as a roto-translational movement evolving in an earthflow. It developed within a catchment showing high-relief, diffuse outcrops of clay-rich deposits with a high degree of tectonization and tectonic lineaments of regional significance.

Geophysical data suggest that the sliding surface of the initial slope failure phenomena has a thickness of about 25 m, as inferred from the reconstruction of the bedrock depth in the S-wave velocity profiles. A major reactivation event in the middle and lower sectors of the wider complex landslide was observed in the 1974 stereo-pairs, which was related to a heavy rainfall event occurred in January of 1972. Such a long period of heavy precipitation could have promoted a rise in water level and/or a saturation of the surface layer within a deformation zone with a limited maximum thickness of about 4–5 m. Our investigation

suggests that the active landslide area still shows evident signs of activity, although with a general trend of decrease in activity. As a matter of fact, the shorter-term evolution from the UAV surveys is mainly due to a retrogression of the active scarp, lateral shallow movements, and a toe advancement.

Our results can be useful for landscape modeling, the evaluation of geomorphological hazard and risk, and quantitative geomorphological analysis of slope processes. We remark that the detailed reconstruction of the evolution of complex slow-moving landslides requires the integration of multidisciplinary data. In particular, multi-decadal landslide mapping and estimation of activity maps are important tools for the analysis of possible threshold of rainfall events and can be effectively combined with seismic data to reconstruct the thickness of the present-day active landslide body, the water-table level and the geometry of the deeper and older sliding surface. Finally, it should be emphasized that the collected seismic data and in particular the single-offset multicomponent MASW showed a great potential and can represent an effective and powerful method for characterizing the 2-D geometry of large landslides.

Author contributions All authors contributed to the study conception and design. Material preparation, data collection and analysis were performed by Dario Gioia, Giuseppe Corrado, Antonio Minervino Amodio, and Marcello Schiattarella. The first draft of the manuscript was written by Dario Gioia and all authors commented on previous versions of the manuscript. All authors read and approved the final manuscript.

Funding Open access funding provided by Consiglio Nazionale Delle Ricerche (CNR) within the CRUI-CARE Agreement. The authors declare that no funds, grants, or other support were received during the preparation of this manuscript.

Declarations

Conflict of interest The authors have no relevant financial or non-financial interests to disclose.

Open Access This article is licensed under a Creative Commons Attribution 4.0 International License, which permits use, sharing, adaptation, distribution and reproduction in any medium or format, as long as you give appropriate credit to the original author(s) and the source, provide a link to the Creative Commons licence, and indicate if changes were made. The images or other third party material in this article are included in the article's Creative Commons licence, unless indicated otherwise in a credit line to the material. If material is not included in the article's Creative Commons licence and your intended use is not permitted by statutory regulation or exceeds the permitted use, you will need to obtain permission directly from the copyright holder. To view a copy of this licence, visit <http://creativecommons.org/licenses/by/4.0/>.

References

- Alonso-Pandavenes O, Torrijo FJ, Garzón-Roca J, Gracia A (2023) Early investigation of a landslide sliding surface by HVSR and VES geophysical techniques combined a case study in guarumales (Ecuador). *Appl Sci (switzerland)* 13:1023. <https://doi.org/10.3390/app13021023>
- Arai H, Tokimatsu K (2005) S-Wave velocity profiling by joint inversion of microtremor dispersion curve and horizontal-to-vertical (H/V) spectrum. *B Seismol Soc Am* 95:1766–1778. <https://doi.org/10.1785/0120040243>
- Ardizzone F, Bucci F, Cardinali M, Fiorucci F, Pisano L, Santangelo M, Zumpano V (2023) Geomorphological landslide inventory map of the daunia apennines, southern Italy. *Earth Syst Sci Data* 15:753–767. <https://doi.org/10.5194/essd-15-753-2023>
- Aringoli D, Gentili B, Materazzi M, Pambianchi G, Sciarra N (2013) DSGSDs induced by post-glacial decompression in Central Apennine (Italy). In: *Landslide science and practice: global environmental change*. Springer, Berlin, pp 417–423

- Bekler T, Ekinci YL, Demirci A, Erginal AE, Ertekin C (2011) Characterization of a landslide using seismic refraction, electrical resistivity and hydrometer methods, adatepe-çanakkale, nw turkey. *J Environ Eng Geophys* 16:115–126. <https://doi.org/10.2113/JEEG16.3.115>
- Bertolini G, Corsini A, Tellini C (2017) Fingerprints of large-scale landslides in the landscape of the emilia apennines. In: Soldati M, Marchetti M (eds) *Landscapes and landforms of Italy*. Springer, Cham, pp 215–224. https://doi.org/10.1007/978-3-319-26194-2_18
- Borgomeo E, Hebditch KV, Whittaker AC, Lonergan L (2014) Characterising the spatial distribution, frequency and geomorphic controls on landslide occurrence Molise, Italy. *Geomorphology* 226:148–161. <https://doi.org/10.1016/j.geomorph.2014.08.004>
- Calò F, Calcaterra D, Iodice A, Parise M, Ramondini M (2012) Assessing the activity of a large landslide in southern Italy by ground-monitoring and SAR interferometric techniques. *Int J Remote Sens* 33:3512–3530. <https://doi.org/10.1080/01431161.2011.630331>
- Capizzi P, Martorana R (2014) Integration of constrained electrical and seismic tomographies to study the landslide affecting the cathedral of Agrigento. *J Geophys Eng*. <https://doi.org/10.1088/1742-2132/11/4/045009>
- Casagli N, Frodella W, Morelli S, Tofani V, Ciampalini A, Intrieri E, Raspini F, Rossi G, Tanteri L, Lu P (2017) Spaceborne, UAV and ground-based remote sensing techniques for landslide mapping, monitoring and early warning. *Geoenviron Disasters*. <https://doi.org/10.1186/s40677-017-0073-1>
- Conforti M, Muto F, Rago V, Critelli S (2014) Landslide inventory map of north-eastern Calabria (South Italy). *J Maps* 10:90–102. <https://doi.org/10.1080/17445647.2013.852142>
- Cotecchia F, Vitone C, Santaloia F, Pedone G, Bottiglieri O (2015) Slope instability processes in intensely fissured clays: case histories in the Southern Apennines. *Landslides* 12:877–893. <https://doi.org/10.1007/s10346-014-0516-7>
- Cruden DM, Varnes DJ (1996) Landslide types and processes. In: Turner AK, Shuster RL (eds) *Landslides: investigation and Mitigation*. National Academies Press, Washington, pp 36–75
- Dal Moro G (2014) Surface wave analysis for near surface applications. Elsevier, New York. <https://doi.org/10.1016/C2013-0-18480-2>
- Dal Moro G (2019a) Effective active and passive seismics for the characterization of urban and remote areas: four channels for seven objective functions. *Pure Appl Geophys* 176:1445–1465. <https://doi.org/10.1007/s00024-018-2043-2>
- Dal Moro G (2019b) Surface wave analysis: improving the accuracy of the shear-wave velocity profile through the efficient joint acquisition and full velocity spectrum (FVS) analysis of rayleigh and love waves. *Explor Geophys* 50:408–419. <https://doi.org/10.1080/08123985.2019.1606202>
- Dal Moro G (2020) Efficient joint analysis of surface waves and introduction to vibration analysis: beyond the clichés. Springer, Cham
- Dal Moro G (2023) MASW? A critical perspective on problems and opportunities in surface-wave analysis from active and passive data (with few legal considerations). *Phys Chem Earth Parts a/b/c* 130:103369. <https://doi.org/10.1016/j.pce.2023.103369>
- Dal Moro G, Ferigo F (2011) Joint analysis of rayleigh and Love-wave dispersion: issues, criteria and improvements. *J Appl Geophys* 75:573–589. <https://doi.org/10.1016/j.jappgeo.2011.09.008>
- Dal Moro G, Al-Arifi N, Moustafa SR (2019) On the efficient acquisition and holistic analysis of Rayleigh waves: technical aspects and two comparative case studies. *Soil Dyn Earthq Eng*. <https://doi.org/10.1016/j.soildyn.2019.105742>
- Di Maio C, Fornaro G, Gioia D, Reale D, Schiattarella M, Vassallo R (2018) In situ and satellite long-term monitoring of the Latronico landslide, Italy: displacement evolution, damage to buildings, and effectiveness of remedial works. *Eng Geol* 245:218–235. <https://doi.org/10.1016/j.enggeo.2018.08.017>
- Giordan D, Allasia P, Manconi A, Baldo M, Santangelo M, Cardinali M, Corazza A, Albanese V, Lolli G, Guzzetti F (2013) Morphological and kinematic evolution of a large earthflow: the Montaguto landslide, southern Italy. *Geomorphology* 187:61–79. <https://doi.org/10.1016/j.geomorph.2012.12.035>
- Guzzetti F, Mondini AC, Cardinali M, Fiorucci F, Santangelo M, Chang KT (2012) Landslide inventory maps: new tools for an old problem. *Earth Sci Rev* 112:42–66. <https://doi.org/10.1016/j.earscirev.2012.02.001>
- Himi M, Anton M, Sendrós A, Abancó C, Ercoli M, Lovera R, Deidda GP, Urruela A, Rivero L, Casas A (2022) Application of resistivity and seismic refraction tomography for landslide stability assessment in valcebre, Spanish Pyrenees. *Remote Sens-Basel* 14:6333. <https://doi.org/10.3390/rs14246333>
- Hu X, Burgmann R, Schulz WH, Fielding EJ (2020) Four-dimensional surface motions of the Slumgullion landslide and quantification of hydrometeorological forcing. *Nat Commun* 11:2792. <https://doi.org/10.1038/s41467-020-16617-7>
- Hunter JA et al (2022) Seismic site characterization with shear wave (SH) reflection and refraction methods. *J Seismol* 26:631–652. <https://doi.org/10.1007/s10950-021-10042-z>

- Hussain Y et al (2019) Multiple geophysical techniques for investigation and monitoring of Sobradinho Landslide, Brazil. *Sustainability* (switzerland) 11:6672. <https://doi.org/10.3390/su11236672>
- Imani P, Abd El-Raouf A, Tian G (2021) Landslide investigation using seismic refraction tomography method: a review. *Ann Geophys.* <https://doi.org/10.4401/AG-8633>
- Imposa S, Grassi S, Fazio F, Rannisi G, Cino P (2017) Geophysical surveys to study a landslide body (north-eastern Sicily). *Nat Hazards* 86:327–343. <https://doi.org/10.1007/s11069-016-2544-1>
- Irham MN, Yulianto T, Yuliyanto G, Widada S (2021) Estimation of landslide prone zones around the Semarang Fault based on by combining the slope stability analysis and HVSR microtremor methods. *J Phys Conf Ser.* <https://doi.org/10.1088/1742-6596/1943/1/012032>
- James MR, Chandler JH, Eltner A, Fraser C, Miller PE, Mills JP, Noble T, Robson S, Lane SN (2019) Guidelines on the use of structure-from-motion photogrammetry in geomorphic research. *Earth Surf Proc Land* 10:2081–2084. <https://doi.org/10.1002/esp.4637>
- Lacroix P, Handwerker AL, Bièvre G (2020) Life and death of slow-moving landslides. *Nat Rev Earth Environ* 1:404–419. <https://doi.org/10.1038/s43017-020-0072-8>
- Lazzari M, Gioia D (2016) Regional-scale landslide inventory, central-western sector of the Basilicata region (Southern Apennines, Italy). *J Maps* 12:852–859. <https://doi.org/10.1080/17445647.2015.1091749>
- Lazzari M, Gioia D, Anzidei B (2018) Landslide inventory of the basilicata region (Southern Italy). *J Maps* 14:348–356. <https://doi.org/10.1080/17445647.2018.1475309>
- Leonelli G, Chelli A (2024) Spatial distribution patterns of dated landslide events in the Northern Apennines in response to Holocene regional climatic changes. *CATENA.* <https://doi.org/10.1016/j.catena.2023.107705>
- Mazzanti P, Caporossi P, Brunetti A, Mohammadi FI, Bozzano F (2021) Short-term geomorphological evolution of the Poggio Baldi landslide upper scarp via 3D change detection. *Landslides* 18:2367–2381. <https://doi.org/10.1007/s10346-021-01647-z>
- Mercuri M, Conforti M, Ciurleo M, Borrelli L (2023) UAV application for short-time evolution detection of the vomice landslide (South Italy). *Geosciences.* <https://doi.org/10.3390/geosciences13020029>
- Minervino Amodio A, Aucelli PPC, Garfi V, Roskopf CM (2020) Digital photogrammetric analysis approaches for the realization of detailed terrain models. *Rend Online Societa Geologica Italiana* 52:69–75. <https://doi.org/10.3301/ROL.2020.21>
- Nakamura Y (1989) A method for dynamic characteristics estimation of subsurface using microtremor on the ground surface Railway Technical Research Institute. *Q Rep* 30:25–33
- Pánek T (2014) Recent progress in landslide dating. *Prog Phys Geogr Earth Environ* 39:168–198. <https://doi.org/10.1177/0309133314550671>
- Parise M, Federico A, Palladino G (2012) Historical evolution of multi-source mudslides. In: Eberhardt E, Froese C, Turner AK, Lerouil S (eds) *Landslides and engineered slopes. Protecting society through improved understanding. Proceedings 11th international symposium on landslides, Banff (Canada), 3–8 June 2012, vol 1, pp 401–407*
- Parise M, Wasowski J (1999) Landslide activity maps for the evaluation of landslide hazard: three case studies from Southern Italy. *Nat Hazards* 20:159–183. <https://doi.org/10.1023/a:1008045127240>
- Park CB, Miller RD, Xia J (1999) Multichannel analysis of surface waves. *Geophysics* 64:800–808. <https://doi.org/10.1190/1.1444590>
- Peduto D, Santoro M, Aceto L, Borrelli L, Gullà G (2021) Full integration of geomorphological, geo-technical, A-DInSAR and damage data for detailed geometric-kinematic features of a slow-moving landslide in urban area. *Landslides* 18:807–825. <https://doi.org/10.1007/s10346-020-01541-0>
- Pescatore T, Renda P, Schiattarella M, Tramutoli M (1999) Stratigraphic and structural relationships between Meso-Cenozoic Lagonegro basin and coeval carbonate platforms in southern Apennines, Italy. *Tectonophysics* 315:269–286. [https://doi.org/10.1016/S0040-1951\(99\)00278-4](https://doi.org/10.1016/S0040-1951(99)00278-4)
- Pisano L, Zumpano V, Malek Ž, Roskopf CM, Parise M (2017) Variations in the susceptibility to landslides, as a consequence of land cover changes: a look to the past, and another towards the future. *Sci Total Environ* 601–602:1147–1159. <https://doi.org/10.1016/j.scitotenv.2017.05.231>
- Riviello A, Schiattarella M, Vaccaro MP (1997) Geological structure of the Tolve area, Basilicata, southern Apennines, as inferred from surface and subsurface data. *Alp Mediterr Quat* 10:557–561
- Samyn K, Travelletti J, Bitri A, Grandjean G, Malet JP (2012) Characterization of a landslide geometry using 3D seismic refraction traveltime tomography: the La valette landslide case history. *J Appl Geophys* 86:120–132. <https://doi.org/10.1016/j.jappgeo.2012.07.014>
- Santangelo M, Gioia D, Cardinali M, Guzzetti F, Schiattarella M (2013) Interplay between mass movement and fluvial network organization: an example from southern Apennines, Italy. *Geomorphol* 188:54–67. <https://doi.org/10.1016/j.geomorph.2012.12.008>

- Santangelo M, Gioia D, Cardinali M, Guzzetti F, Schiattarella M (2015) Landslide inventory map of the upper Sinni River valley. *South Italy J Maps* 11:444–453. <https://doi.org/10.1080/17445647.2014.949313>
- Santangelo M, Zhang L, Rupnik E, Deseilligny MP, Cardinali M (2022) Landslide evolution pattern revealed by multi-temporal DSMS obtained from historical aerial images. In: *International archives of the photogrammetry, remote sensing and spatial information sciences—ISPRS Archives*, 2022, pp 1085–1092. <https://doi.org/10.5194/isprs-archives-XLIII-B2-2022-1085-2022>
- Sass O, Bell R, Glade T (2008) Comparison of GPR, 2D-resistivity and traditional techniques for the sub-surface exploration of the Öschingen landslide, Swabian Alb (Germany). *Geomorphology* 93:89–103. <https://doi.org/10.1016/j.geomorph.2006.12.019>
- Schiattarella M, Giano SI, Gioia D (2017) Long-term geomorphological evolution of the axial zone of the Campania-Lucania Apennine, southern Italy: a review. *Geol Carpath* 68:57–67. <https://doi.org/10.1515/geoca-2017-0005>
- Soeters R, van Westen CJ (1996) Slope instability recognition, analysis, and zonation. In: Turner AK, Schuster RL (eds) *Landslides: investigation and mitigation transp res board sp rep 247*. The National Academies Press, WA, pp 129–177
- Spalluto L, Fiore A, Miccoli MN, Parise M (2021) Activity maps of multi-source mudslides from the Daunia Apennines (Apulia, southern Italy). *Nat Hazards* 106:277–301. <https://doi.org/10.1007/s11069-020-04461-3>
- Stucchi E, Ribolini A, Anfuso A (2013) High-resolution reflection seismic survey at the Patigno landslide, Northern Apennines Italy. *Near Surface Geophys*. <https://doi.org/10.3997/1873-0604.2013036>
- Trigila A, Iadanza C, Spizzichino D (2010) Quality assessment of the Italian Landslide Inventory using GIS processing. *Landslides* 7:455–470. <https://doi.org/10.1007/s10346-010-0213-0>
- van Westen CJ, Lulie Getahun F (2003) Analyzing the evolution of the Tessina landslide using aerial photographs and digital elevation models. *Geomorphology* 54:77–89. [https://doi.org/10.1016/s0169-555x\(03\)00057-6](https://doi.org/10.1016/s0169-555x(03)00057-6)
- Whiteley JS et al (2020) Landslide monitoring using seismic refraction tomography – The importance of incorporating topographic variations. *Eng Geol* 268. <https://doi.org/10.1016/j.enggeo.2020.105525>
- Widyadarsana SN, Hartantyo E (2021) Lithological modelling based on shear wave velocity using horizontal to vertical spectral ratio (HVSr) inversion of ellipticity curve method to mitigate landslide hazards at the main road Of Samigaluh District, Kulon Progo Regency, Yogyakarta. In: *E3S Web of conferences*, 2021. <https://doi.org/10.1051/e3sconf/202132501009>
- Wróbel M, Stan-Kłeczek I, Marciniak A, Majdański M, Kowalczyk S, Nawrot A, Cader J (2023) Integrated geophysical imaging and remote sensing for enhancing geological interpretation of landslides with uncertainty estimation—a case study from cisiec Poland. *Remote Sens-Basel* 15:238. <https://doi.org/10.3390/rs15010238>

Publisher's Note Springer Nature remains neutral with regard to jurisdictional claims in published maps and institutional affiliations.